ACS APPLIED MATERIALS & INTERFACES

Research Article

www.acsami.org

Development of Nanofiber Sponges-Containing Nerve Guidance Conduit for Peripheral Nerve Regeneration in Vivo

Binbin Sun,[†] Zifei Zhou,[‡] Tong Wu,[†] Weiming Chen,[†] Dawei Li,[†] Hao Zheng,[†,§] Hany El-Hamshary,[∥,⊥] Salem S. Al-Deyab,[∥] Xiumei Mo,[*,†,#] and Yinxian Yu[*,‡]

[†]State Key Lab for Modification of Chemical Fibers & Polymer Materials, College of Chemistry, Chemical Engineering and Biotechnology, Donghua University, Shanghai 201620, China

[‡]Department of Orthopaedic Surgery, Shanghai General Hospital, Shanghai Jiao Tong University School of Medicine, Shanghai 200080, China

[§]State Key Laboratory of Polymer Materials Engineering, Sichuan University, Chengdu 610065, China

[∥]Department of Chemistry, College of Science, King Saud University, Riyadh 11451, Kingdom of Saudi Arabia

[⊥]Department of Chemistry, Faculty of Science, Tanta University, Tanta 31527, Egypt

[#]Shandong International Biotechnology Park Development Company, Ltd., Yantai 264003, China

ABSTRACT: In the study of hollow nerve guidance conduit (NGC), the dispersion of regenerated axons always confused researchers. To address this problem, filler-containing NGC was prepared, which showed better effect in the application of nerve tissue engineering. In this study, nanofiber sponges with abundant macropores, high porosity, and superior compressive strength were fabricated by electrospinning and freeze-drying. Poly(L-lactic acid-*co*-ε-caprolactone)/silk fibroin (PLCL/SF) nanofiber sponges were used as filler to prepare three-dimensional nanofiber sponges-containing (NS-containing) NGC. In order to study the effect of fillers for nerve regeneration, hollow NGC was set as control. In vitro cell viability studies indicated that the NS-containing NGC could enhance the proliferation of Schwann cells (SCs) due to the macroporous structure. The results of hematoxylin−eosin (HE) and immunofluorescence staining confirmed that SCs infiltrated into the nanofiber sponges. Subsequently, the NS-containing NGC was implanted in a rat sciatic nerve defect model to evaluate the effect in vivo. NS-containing NGC group performed better in nerve function recovery than hollow NGC group. In consideration of the walking track and triceps weight analysis, NS-containing NGC was close to the autograft group. In addition, histological and morphological analyses with HE and toluidine blue (TB) staining, and transmission electron microscope (TEM) were conducted. Better nerve regeneration was observed on NS-containing NGC group both quantitatively and qualitatively. Furthermore, the results of three indexes' immuno-histochemistry and two indexes' immunofluorescence all indicated good nerve regeneration of NS-containing NGC as well, compared with hollow NGC. The results demonstrated NS-containing NGC had great potential in the application of peripheral nerve repair.

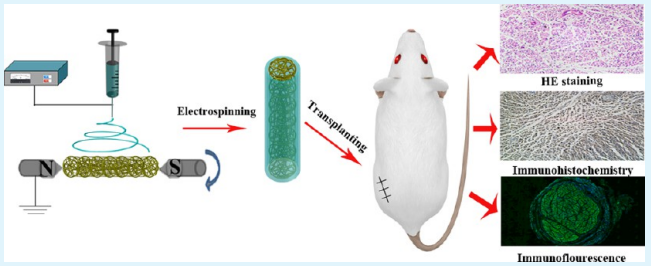

KEYWORDS: *nerve regeneration, electrospinning, nanofiber sponges, nerve guidance conduit, poly(L-lactic acid-co-ε-caprolactone) (PLCL), silk fibroin (SF)*

1. INTRODUCTION

Peripheral nerve injury is a common clinical problem, which has a high morbidity of the trauma patients.[1−3] Nerve tissue engineering scaffold, also called nerve guidance conduit (NGC) with a cylindrical tube shape, has been fabricated to guide cells proliferation and facilitate axons extension of injured neural tissues in three dimensions.[4,5] In previous study, NGC played the role of biomimic extracellular matrix (ECM) for Schwann cells (SCs) adhesion and growth at the beginning.[6] Security, biocompatibility, biodegradability, permeability, mechanical strength, and similarity structure to ECM is quite essential for an ideal NGC.

In the past decade, various NGCs were fabricated to guide neural regeneration. Initially, NGC with a single hollow lumen was designed to guide neural regeneration. However, studies indicated that hollow NGC will lead to the dispersion of regenerating axons during nerve regeneration. And the dispersion of regeneration across the NGC tube may lead to misdirection and polyinnervation.[7−9] Therefore, some complex NGCs have been developed with the incorporation of physical fillers into the NGC lumen to mimic the endoneurial-like structure of autologous nerve grafts. A series of biomaterial-based filler has been included into the lumen of NGC to guide nerve regeneration, such as fibers,[10] filaments,[11] and gels.[12]

Received: May 12, 2017
Accepted: July 18, 2017
Published: July 18, 2017

DOI: 10.1021/acsami.7b06707
ACS Appl. Mater. Interfaces 2017, 9, 26684−26696

Lundborg and Kanje first reported silicone conduits with eight nylon filaments filled in the application of 10 mm rat model.[13] Later, in Matsumoto's study, NGC was made of a poly(glycolic acid (PGA)−collagen tube filled with laminin-coated collagen fibers and was used to bridge an 80 mm gap in the left peroneal nerve of a beagle dog. In the time frame 10−12 months after implantation, the pattern of walking was restored to almost normal.[10] Although the mechanism has not yet been verified due to the difficulty of a meticulous imitation of the in vivo situation, filler-containing NGC shows potential to promote nerve regeneration.[14] However, the above-mentioned reports focused on the aligned filler containing for NGC; few sponge fillers with irregular morphology were used in the preparation of NGC.

Currently, electrospinning was a general method to prepare tissue engineering scaffolds including nerve, skin, vascular, bone, and so on.[15,16] Electrospun tissue engineering scaffold could offer ECM-mimicking nanoscale structure with high specific surface and porosity. However, the disadvantages of electrospinning restricted its applications. (1) Most of electrospun scaffold is a membrane with two-dimensional (2D) structure. Fabricating a 3D nanofiber scaffold rather than the conventional 2D membrane is still a major research direction.[17] (2) The pore size of electrospun scaffold is too small for cells to infiltrate into the nanofiber scaffold.[18] To solve these problems, Fong et al. produced 3D nanofibrous scaffold by two steps: (1) the electrospun polycaprolactone (PCL) nanofibers were broken with immersion into liquid nitrogen; (2) then the 3D nanofibrous scaffold was prepared by thermally induced self-agglomeration.[19] However, the process of 3D PCL nanofibrous scaffold was too complicated to process heavily. On the other hand, PCL was hydrophobic; thus the scaffold was not suitable for cell colonization.[20] In the study of Chen et al., gelatin and poly(lactic acid) (PLA) were mixed to prepare electrospun nanofiber membranes. Then, electrospun gelatin/PLA nanofiber was dispersed, freeze-dried, and heat-treated to fabricate a 3D nanofiber scaffold. It was confirmed that the 3D nanofiber scaffold can not only keep the nanofibrous structure but also possess some merits: such as macroporous structure for cell infiltration, high compressive strength, and high porosity.[21] In vitro and in vivo experiments indicated that this 3D nanofiber scaffold could promote the regeneration of cartilage tissue.[22] It is suggested that there is potential of gelatin/PLA 3D nanofiber scaffold for cartilage tissue engineering by combining electrospinning and freeze-drying. Herein, the promising electrospun composites of poly(L-lactic acid-*co*-ε-caprolactone)/silk fibroin (PLCL/SF) were used.[23,24] A 3D nanofiber nerve scaffold was fabricated with PLCL and SF which had macroporous structure for cells growth, high porosity, and enough mechanical properties.

In this study, 3D nanofiber sponges were fabricated via dispersion and freeze-drying. The 3D nanofiber sponges were set as filler to prepare nanofiber sponges-containing NGC (NS-containing NGC). This nanofiber sponges-containing NGC could provide a 3D microenvironment with macropores for SCs growth and infiltration. It could also biomimic the endoneurial-like architecture of nerve fascicles. Morphology and mechanical properties of NS-containing NGC were characterized. Furthermore, the in vitro and in vivo experiments have been performed to evaluate the biocompatibility and promotion for nerve regeneration.

2. EXPERIMENTAL SECTION

2.1. Materials. Copolymer PLCL (Mw = 300 kDa; LA:CL = 75:25) was purchased from Jinan Daigang Co., Ltd. (China). Bombyxmori silkworm cocoons were supplied by Jiaxing Silk Co., Ltd. (China), 1,1,1,3,3,3-Hexafluoro-2-propanol (HFIP) was purchased from Alfa Aesar Co. (Ward Hill, MA, USA). *tert*-Butanol and glutaraldehyde were obtained from Shanghai Aladdin Bio-Chem Technology Co., Ltd. (China); both of them were analytical grade reagents. Cell culture reagents, such as Dulbecco's modified Eagle's medium (DMEM), fetal bovine serum, and trypsin were purchased from Life Technologies (Waltham, MA, USA). SCs (rat) were obtained from the Shanghai Institute of Biochemistry and Cell Biology (SIBCB, CAS, China).

2.2. Fabrication of PLCL/SF Nanofiber Membranes. The regenerated SF was prepared according to the previously reported method.[25] The electrospinning solution (w/v (%) = 8) was prepared by mixing PLCL and SF (w/w (%) = 20:80) in HFIP and stirring at room temperature for 4 h. PLCL/SF nanofiber membranes were fabricated by electrospinning process as was done previously.[26] In brief, PLCL/SF solution was placed in 5 mL plastic syringes loaded in syringe pumps (789100C, Cole-Parmer Instruments, USA) and operated at the rate of 1 mL/h. PLCL/SF solution was electrospun with a syringe equipped with a 21G steel needle using a voltage of 12 kV high-voltage power supply (BGG6-358, BMEI Co. Ltd., China). Aluminum foil (5 × 5 mm^2) was used as a collector, and the distance between needle and collector was 5−6 cm. All of the collected PLCL/SF nanofiber membranes were placed in vacuum overnight to remove the residual solvent.

2.3. Preparation of PLCL/SF 3D Nanofiber Sponges. PLCL/SF 3D nanofiber sponges were prepared with the method shown in Figure 1A. In brief, PLCL/SF nanofiber membranes were cut into small pieces (0.5 cm × 0.5 cm), which were immersed into *tert*-butanol solution to disperse with homogenizer (IKA T-18, Germany) at the speed of 10000 rpm for 30 min. Then, the dispersed nanofibers were poured into a 24-well cell culture plate and freeze-dried for 24 h. Freeze-dried 3D nanofiber sponges (un-cross-linked) were cross-linked via glutaraldehyde vapor for 20 min. Eventually, cross-linked nanofiber sponges were placed in vacuum overnight to remove the residual solvent and obtain the PLCL/SF 3D nanofiber sponges (cross-linked).

2.4. Characterization of PLCL/SF 3D Nanofiber Sponges. The morphology of PLCL/SF nanofiber membrane, freeze-dried 3D nanofiber sponge (un-cross-linked), and PLCL/SF 3D nanofiber sponge (cross-linked) were examined using a digital camera (Canon 550D, Japan) and scanning electron microscope (SEM, Hitachi TM-100, Japan), respectively. The corresponding pore size distribution of three samples was calculated by a CFP-1100-AI capillary flow porometer (PMI, Porous Materials Inc.).

The total porosity (%) of the different samples was determined via liquid displacement.[27] Briefly, each sample with a known dry weight was placed in absolute acetone for 48 h. Acetone was used due to its ability to permeate through the scaffolds without swelling or shrinking the matrix. The total amount of acetone that the scaffolds were able to absorb during 48 h was calculated by the following equation:

$$\text{porosity}\ (\%) = \frac{W_w - W_d}{\rho_a V_s} \times 100$$

where W_w (g) and W_d (g) represent wet weight and dry weight of the samples, respectively, ρ_a (g/cm^3) is the density of acetone at room temperature, and V_s (cm^3) represents the volume of the wet sample. Each sample was measured at least five times (n = 5) repeatedly to obtain the average values.

Pore size distributions of three samples were measured by through-pore size analyzer (Quantachrome Instruments, USA). To analyze the mechanical properties of PLCL/SF nanofiber sponges, cyclic compression experiments were conducted by a compression testing machine (HY-940FS, China). Samples have been composed with 100 cycles and five replicates (n = 5).

DOI: 10.1021/acsami.7b06707
ACS Appl. Mater. Interfaces 2017, 9, 26684−26696

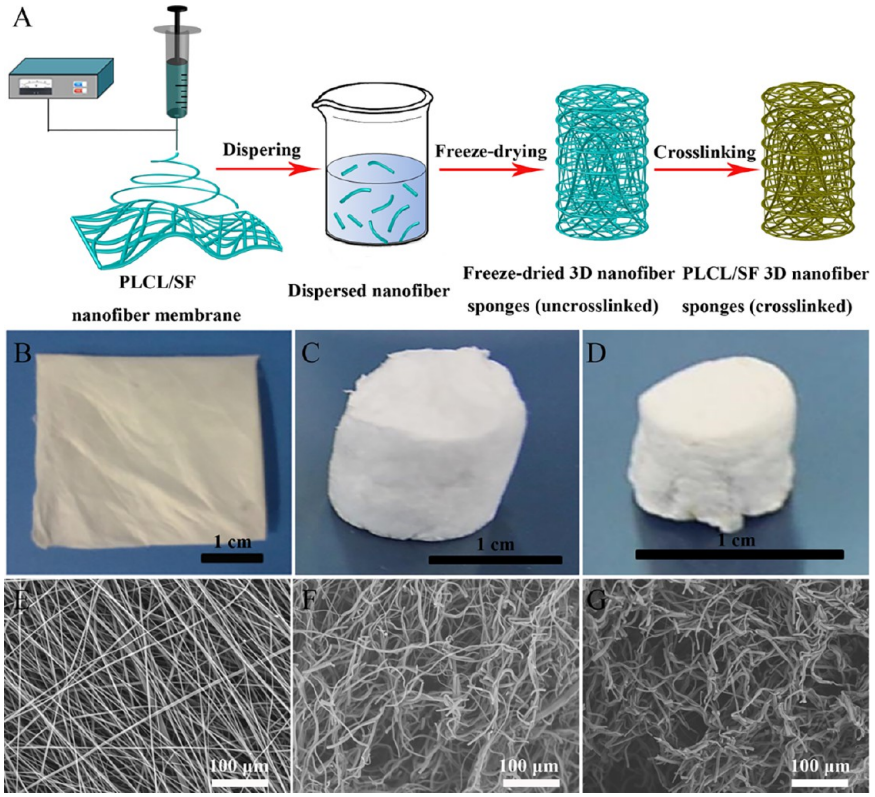

Figure 1. (A) Schematic illustration of PLCL/SF 3D nanofiber sponges by electrospinning and freeze-drying methods. Digital photographs of (B) PLCL/SF nnaofiber membrane, (C) freeze-dried 3D nanofiber sponges, and (D) PLCL/SF 3D nanofiber sponges. SEM images of (E) PLCL/SF nnaofiber membrane, (F) freeze-dried 3D nanofiber sponges, and (G) PLCL/SF 3D nanofiber sponges.

2.5. Preparation and Characterization of PLCL/SF NS-Containing NGC. Sponge-containing NGC could guide the extension of nerve axons. Herein, PLCL/SF 3D nanofiber sponges were used as filler to prepare nanofiber NS-containing NGC. (1) Cross-linked PLCL/SF nanofiber sponges were fabricated in tubular structure (length, 50 mm; diameter, 2 mm) as previously described.[26] (2) New nanofiber (PLCL/SF, w/w (%) = 75:25) was warped on the surface of nanofiber sponges tube by electrospinning to obtain NS-containing NGC. As control, a poly(tetrafluoroethylene) (PTFE) stick (l = 50 mm, Φ = 2 mm) was set as a collector, which was removed after electrospinning (the material is PLCL/SF, w/w (%) = 75:25) to fabricate a hollow NGC.

The cross-section morphology of NS-containing NGC and hollow NGC was characterized by SEM, and the axial compressive mechanical properties of two NGCs were evaluated with cyclic compression experiment.

2.6. SC Cells Proliferation and Infiltration in NS-Containing NGC. In order to analyze the biocompatibility of PLCL/SF NS-containing NGC, SCs were cultured on the NS-containing NGC, the hollow NGC, and tissue culture plate (TCP). SC cells were cultured in DMEM medium supplemented with 10% fetal bovine serum (FBS) and 1% penicillin−streptomycin formulation at 37 °C with 5% CO_2 in a humidified atmosphere. Samples were cut into 10 mm length and sterilized with 75% ethanol and UV light for 2 h. Then SCs were detached by 0.25% trypsin−EDTA and seeded on the nanofiber sponges' filler of NS-containing NGC, the lumen of hollow NGC, and the surface of TCP with a density of 1×10^4 cells/well, approximately (n = 8). After 1, 3, 5, and 7 days of culture, SC cells viability was determined by CCK-8 assay (Sigma-Aldrich Co., Ltd., USA). During the culturing process, medium was refreshed every other day. After culturing for 7 days, SCs cultured on the NS-containing NGC and hollow NGC were fixed by 4% paraformaldehyde for 2 h at 4 °C. Then, the samples were dehydrated with gradient ethanol solution (50%, 70%, 90%, 95%, and 100%) and observed by SEM at the accelerating voltage of 15 kV.

After culturing for 7 days, NS-containing NGC and hollow NGC were paraffin-embedded, cut in the central (cross and longitudinal), and washed with PBS. After being dewaxed with xylene, some samples were stained with hematoxylin−eosin (HE) staining; some other samples were treated with rabbit anti-S100 antibody (1:100, Sigma, USA) overnight and then stained with rhodamine (TRITC)-labeled goat antirabbit IgG (1:200, Sigma) and 4′,6-diamidino-2-phenylindole (DAPI; 1:200, Life Technologies, USA) for 30 and 5 min, respectively. Subsequently, the HE staining and immunofluorescence staining images were observed through analysis cell infiltration using the inverted fluorescence microscopy (IX71, Olympus, Japan) and confocal laser scanning microscope (CLSM, C2, Nikon, Japan).

2.7. Surgical Procedure. Sprague−Dawley (SD) rats (male or female, 200−250 g) were employed to assess the nerve repairing effect of autograft and various NGCs. All the rats were divided into three groups (autograft, hollow NGC and NS-containing NGC), with each group containing six rats. All the experiments were carried out in accordance to Institutional Animal Care guidelines and approved ethically by the administration committee of experimental animals.

Before the surgical procedure, hollow NGC and NS-containing NGC were sterilized by 75% (v/v) ethanol for 24 h, and the rats were anesthetized by sodium pentobarbital (50 μg/g) and fixed on the operating table. The left leg sciatic nerve of rat was dissected and exposed by a dorsal gluteal muscle splitting. A 10 mm nerve gap was produced by removing the proximal peroneal nerve. In the group of autografts, a 10 mm nerve was excised and rebridged by rotating 180°. At the same time, 10 mm length hollow NGCs and NS-containing NGCs were used to bridge the nerve gap, respectively. During the surgical procedure, autologous nerve and NGCs were secured with 8-0 nylon sutures. After implantation, the implanted site was sterilized and irrigated carefully, and the muscle layer and skin layer were sutured by 4-0 and 2-0 sutures.

2.8. Walking Track Analysis and Triceps Weight Analysis. Four weeks and 12 weeks after implantation, the neurological recovery functions were evaluated through walking track analysis and triceps

DOI: 10.1021/acsami.7b06707
ACS Appl. Mater. Interfaces 2017, 9, 26684−26696

weight analysis. For walking track analysis, both hind plantars were dipped in red ink and the footprints were obtained when the rats moved on the surface of white paper (the dimension was 100 cm × 15 cm). The sciatic function index (SFI) was introduced and calculated according to the following formula by de Medinaceli et al.:[28]

$$\mathrm{SFI} = \frac{109.5(\mathrm{ETS} - \mathrm{NTS})}{\mathrm{NTS}} - \frac{38.3(\mathrm{EPL} - \mathrm{NPL})}{\mathrm{NPL}} - \frac{13.3(\mathrm{EIT} - \mathrm{NIT})}{\mathrm{NIT}} - 8.8$$

where TS, PL, and IT representing toe spread length, paw length, and intermediary toe spread length, respectively, N refers to normal legs, and E refers to experimental legs. The SFI results of each group were calculated at least 3 times ($n = 3$), and herein, SFI = 0 in normal rats for normal sciatic nerve function, while SFI = −100 in the case of rats with a completely severed sciatic nerve.

Triceps surae muscle (TSM) is the target organ of the sciatic nerve. Generally, the TSMs of both sides in each rat were dissected to weigh; then the moist weight was collected in each rat promptly (both in experimental side and normal side). The TSM weight ratio of all animals was calculated as the following equation:

$$\text{TSM weight ratio (\%)} = \frac{\mathrm{TSM(experimental\ leg)}}{\mathrm{TSM(normal\ leg)}}$$

At the same time, the TSMs were paraffin-embedded and sectioned for Masson staining. For the quantitative analysis of the Masson staining, a positive area percentage of collagen was measured using Image-Pro Plus software (Media Cybernetics, Inc., Bethesda, MD, USA)

2.9. Histological Evaluation and Morphological Analysis of Regenerated Nerves. Immediately after nerve function recovery assessment, all the rats were sacrificed The implantation site of the rat sciatic nerve was re-exposed, and the regenerated nerve was harvested for histological evaluation and morphological analysis at 4 and 12 weeks, respectively. Before histological staining, the regenerated nerve tissues were fixed with 4% paraformaldehyde at 4 °C for 24 h. Subsequently, the samples were embedded in paraffin and cut into cross-sections in the middle of specimens. Slices were stained with HE, TB, and LFB, respectively, and which were observed with fluorescence microscopy (IX71, Olympus). The samples were also fixed with 2.5% glutaraldehyde in 4 °C (2 h) for transmission electromicroscope observation. Briefly, the fixed samples were embedded and cut into ultrathin sections and then were stained with lead citrate and uranyl acetate. In the end, the nerve morphology was observed and photographed using transmission electron microscope (TEM; HT7700, Hitachi, Ltd., Japan).

Moreover, the number of positive cells per area (100 μm^2) and myelin positive area were measured through TB staining and LFB staining results via Image-Pro Plus software. The total number of regenerated nerve fibers, myelin thickness, and axon diameter were analyzed by ImageJ software (National Institute of Health, Bethesda, MD, USA).

2.10. Immuno-histochemistry and Immunofluorescence. All slices of regenerated and normal nerve tissues were stained with several antibodies. For immuno-histochemistry, sections were incubated by the primary antibody of rabbit anti S-100 antibody (1:200, Sigma), rabbit anti 200 kDa neurofilament antibody (NF-200, 1:100, Abcam, U.K.), and mouse antiglial fibrillary acidic protein (GFAP; 1:100, CST, USA) respectively. The incubation with primary antibody was kept overnight at 4 °C. Then all the procedures were performed according to the standard protocol.[29] Briefly, the samples were incubated with horseradish peroxidase (HRP)-labeled secondary antibody (DAKO, K5007) for 50 min; then the sections were further processed with the diaminobenzene (DAB) regent kit (DAKO, K5007) for visualization. Finally, the immune stained samples were viewed with the inverted fluorescence microscopy (IX71, Olympus), and quantified the positive area to analyze nerve regeneration.

Immunofluorescence staining was applied to evaluate nerve regeneration. The sections were incubated with S-100 and NF-200 primary antibody, respectively overnight at 4 °C, and then incubated with the secondary antibody of fluorescein isothiocyanate (FITC)-labeled goat antirabbit IgG (1:200, Sigma) and rhodamine (TRITC)-labeled goat antirabbit IgG (1:200, Sigma), respectively. Cell nuclei were stained with DAPI (1:200, Life Technologies) for 5 min. Eventually, the samples were observed on CLSM.

2.11. Statistical Analysis. All the quantitative data were expressed as a mean ± standard deviation. The statistical analysis was carried out using one-way ANOVA, followed by Bonferroni's test for the evaluation of specific differences with Origin 9.1 software (Originlab Corp., Northampton, MA, USA). Only a value of (*) $P < 0.05$ was considered to be significant, and (**) $P < 0.01$ was considered to be highly significant.

3. RESULTS

3.1. Three-Dimensional Nanofiber Sponges' Preparation and Morphology characterization. PLCL/SF nanofiber membranes were fabricated by electrospinning. Then PLCL/SF 3D nanofiber sponges were prepared by dispersing PLCL/SF nanofibers according to the previously described method (Figure 1A). Panels B−D of Figure 1 showed the digital photographs of PLCL/SF nanofiber membrane, freeze-dried 3D nanofiber sponges, and cross-linked PLCL/SF 3D nanofiber spongers. The SEM images were shown in Figure 1E−G, which indicated that three kinds of samples consisted of nanoscale fibers. According to nanofiber diameter analysis, the average nanofiber diameter was 975.51 ± 78.21 (PLCL/SF nanofiber membrane), 1012.25 ± 83.73 (freeze-dried 3D nanofiber sponges), and 987.38 ± 102.01 nm (PLCL/SF 3D nanofiber spongers), indicating no significant differences among all groups.

3.2. Porosity and Mechanical Properties. The porosity of PLCL/SF nanofiber membranes was 72.84 ± 2.93% (Figure 2A). However, when PLCL/SF nanofiber membrane was dispersed to sponge, the porosity increased to 92.21 ± 1.36% (freeze-dried 3D nanofiber sponges) and 88.81 ± 1.13% (PLCL/SF 3D nanofiber spongers). The pore size distribution results documented similar conclusions as well (Figure 2B). The pore size of freeze-dried 3D nanofiber sponges and PLCL/SF 3D nanofiber sponges ranged from 1 to 300 μm and from 1 to 100 μm. Most macroscale pores preformed were higher than 10 μm, while the pore size of PLCL/SF nanofiber membranes ranged from 0.5 to 12 μm and concentrated at 0.5 μm.

Cyclic compression experiment of PLCL/SF 3D nanofiber sponges has been tested to assess the mechanical properties. It was shown that the nanofiber sponges had a good compression recovery capability after cross-linking (maximum 80% strain), and this capability can be maintained even after compressed for 100 times (Figure 2C). The maximum stress and Young's modulus were calculated and have been shown in Figure 2D. The maximum stress of PLCL/SF 3D nanofiber sponges was 376.93 kPa at the first cycle, which decreased to 292.65 kPa at the 50th cycle until to the 100th cycle. The Young's modulus decreased from 28.48 kPa (at first cycle) to 13.27 kPa (at 100th cycle).

3.3. Preparation of NS-Containing NGC. PLCL/SF 3D nanofiber sponges were used as conduit filler to prepare NS-containing NGC (Figure 3A). The length and diameter of NS-containing NGC were 50 mm and 2 mm (Figure 3B). Hollow NGC was fabricated by electrospinning PLCL/SF nanofibers on a PTFE stick with the same size (Figure 3C). The cross-section morphology of NS-containing NGC (Figure 3D,E) and hollow NGC (Figure 3F) were observed by SEM.

3.4. SCs Proliferation and Infiltration. To investigate the biocompatibility, SCs were seeded on NS-containing NGC and cultured for 1, 3, 5, and 7 days. SCs proliferation on TCP and hollow NGC were performed as control. As shown in Figure 4A, CCK-8 assay results performed that SCs showed

DOI: 10.1021/acsami.7b06707
ACS Appl. Mater. Interfaces 2017, 9, 26684−26696

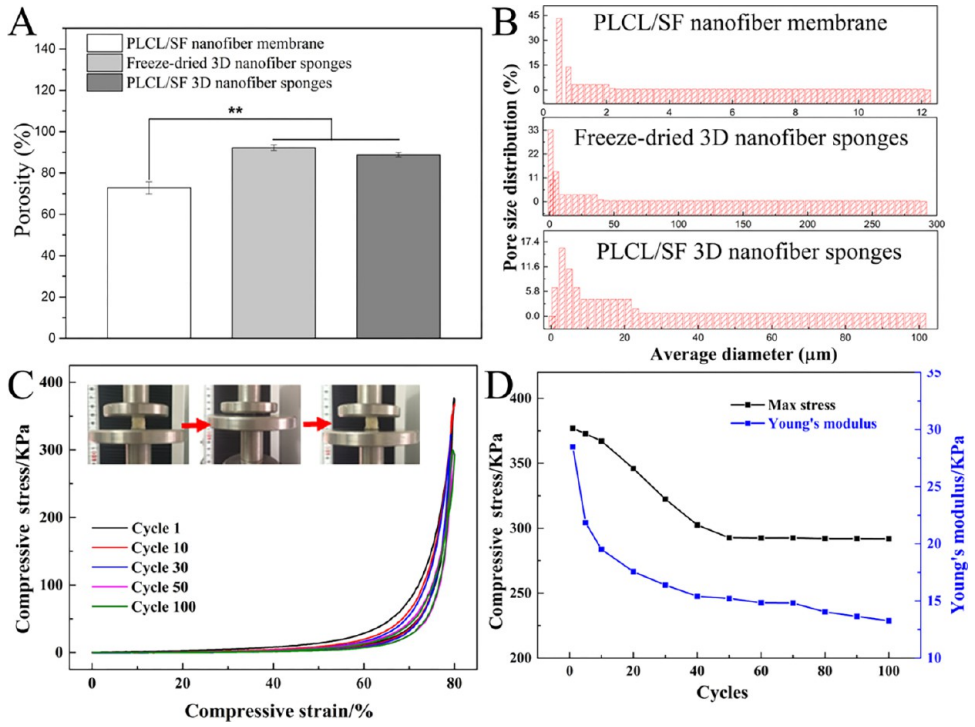

Figure 2. (A) Porosity and (B) pore size distribution of three kinds of scaffolds. (C) Compressive stress−strain curves of PLCL/SF 3D nanofiber sponges with different cycles. Insets: photographs of the PLCL/SF 3D nanofiber sponges under a compressing and releasing cycle (compressive strain = 80%). (D) Max stress and Young's modulus of PLCL/SF 3D nanofiber sponges in 100 cycles.

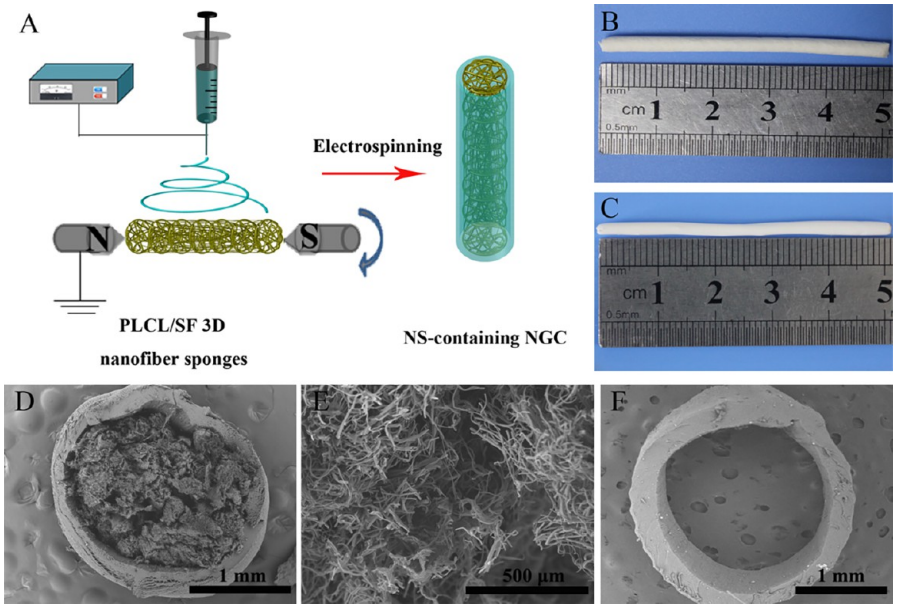

Figure 3. (A) Fabrication schematic illustration of NS-containing NGC by electrospinning. Digital photographs of (B) PLCL/SF 3D nanofiber sponges and (C) NS-containing NGC. Cross-section SEM images of NS-containing NGC in (D) low and (E) high resolution and (F) hollow NGC.

good cell viability on both hollow NGC and NS-containing NGC. It is indicated that both of these two samples were nontoxic. However, on day 1 and day 3, the cell viability on hollow NGC and NS-containing NGC was significantly higher than the TCP control ($P < 0.05$). The difference was increased on day 5 and day 7 ($P < 0.01$). Furthermore, the viability of SCs on NS-containing NGC was significantly higher than hollow NGC on days 5 and 7 ($P < 0.01$). In addition, the cell SEM images indicated that SCs were infiltrated into the sponges (Figure 4B,C).

After culturing for 7 days, two kinds of NGCs were characterized with immunofluorescence (index: S-100) and HE staining after cross-cutting and longitudinal-cutting. As shown in Figure 5, SCs grew on both the inner surface and outer surface of hollow NGC. However, for NS-containing NGC, SCs not only grew on the surface but also infiltrated into the nanofiber sponges. The longitudinal section images of NS-containing NGC showed that SCs could infiltrate into 1000 μm depth after culturing for 7 days.

3.5. Implantation of NGC. NS-containing NGC was implanted into the rat sciatic nerve defect site to investigate the

DOI: 10.1021/acsami.7b06707
ACS Appl. Mater. Interfaces 2017, 9, 26684−26696

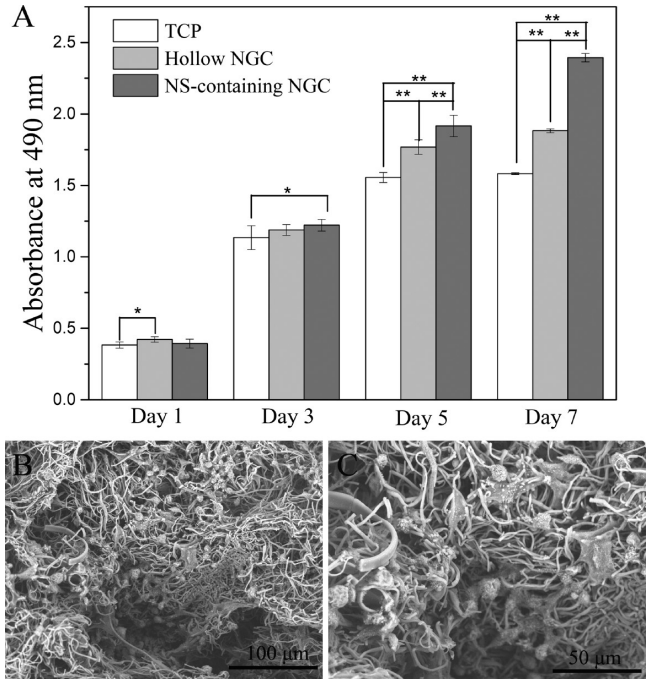

Figure 4. (A) CCK-8 results of SCs cultured on the scaffolds. SEM images of SCs cultured on NS-containing NGC on the seventh day in (B) low and (C) high resolution.

guidance for peripheral nerve regeneration in vivo (Figure 6A), with hollow NGC and autograft implantation performed as control. All of the surgical procedures performed well, and the SD rats survive without any operative complications. The defective rat sciatic nerve in surgery (week 0) and after surgery (weeks 4 and 12) were shown in Figure 6B. Regardless of time, three groups of defective postoperative nerve were rebridged and regenerated successfully.

3.6. Sciatic Nerve Functional Recovery Evaluation. Sciatic nerve functional recovery of SD rats was evaluated by triceps weight analysis and walking track analysis. Besides, the triceps surae muscles (TSMs) of each experimental leg were sectioned for Masson staining (Figure 7A), where red area was muscle cells and blue area was collagen extracellular matrix. The positive area percentage of collagen (with blue color in the images) was measured to evaluate the atrophy of experimented TSMs. As shown in Figure 7B, more collagen was produced on hollow NGC and NS-containing NGC than the autograft group 4 and 12 weeks after implantation ($P < 0.01$). It is suggested that the TSMs of two experimental groups had more serious atrophy than autologous transplantation. The results also displayed that the amount of collagen in NS-containing NGC group was significantly lower than the hollow group ($P < 0.05$). The TSM weight ratio of all animals was calculated and shown in Figure 7C. It was shown that the value of NS-containing NGC was significantly higher than hollow NGC on week 12 ($P < 0.05$), close to the autograft group.

Walking footprints of all SD rats were obtained (Figure 7D), which was used to calculate SFI value with the formula. Figure 7E showed the SFI value of each group, and the SFI value of hollow NGC was much lower than autograft and NS-containing NGC on week 4 ($P < 0.05$) and week 12

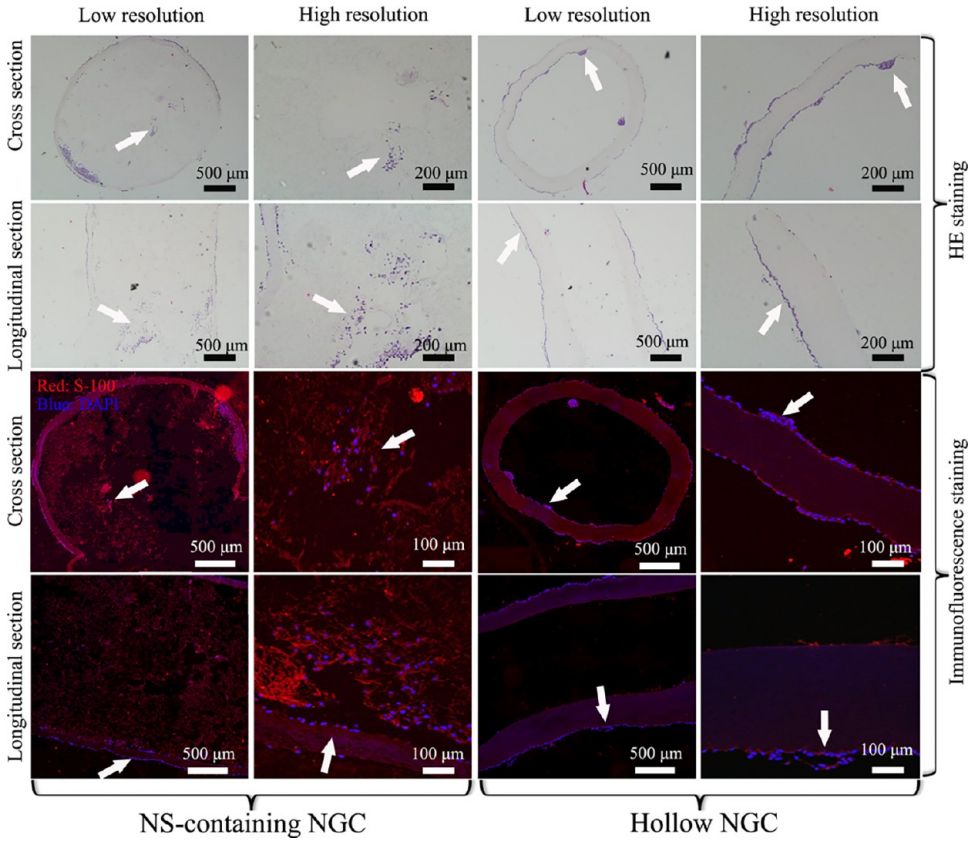

Figure 5. HE and immunofluorescence staining results of SCs cultured on NS-containing NGC and hollow NGC. White arrows tag the same place at low and high magnification.

DOI: 10.1021/acsami.7b06707
ACS Appl. Mater. Interfaces 2017, 9, 26684−26696

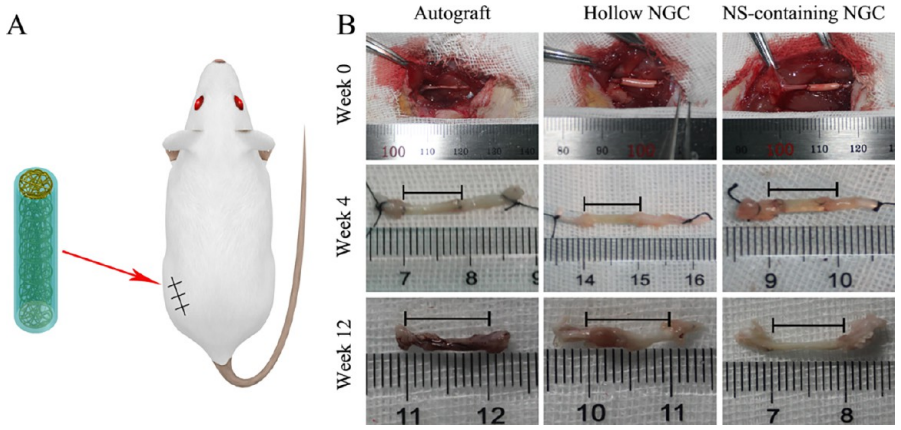

Figure 6. (A) Schematic illustration of transplanting NS-containing NGC into SD rat sciatic nerve defect model. (B) The gross observation of sciatic nerve after surgical procedures at week 0, and the regenerated sciatic nerve after implantation for 4 and 12 weeks (the scale bar = 10 mm, which marked the nerve defect site).

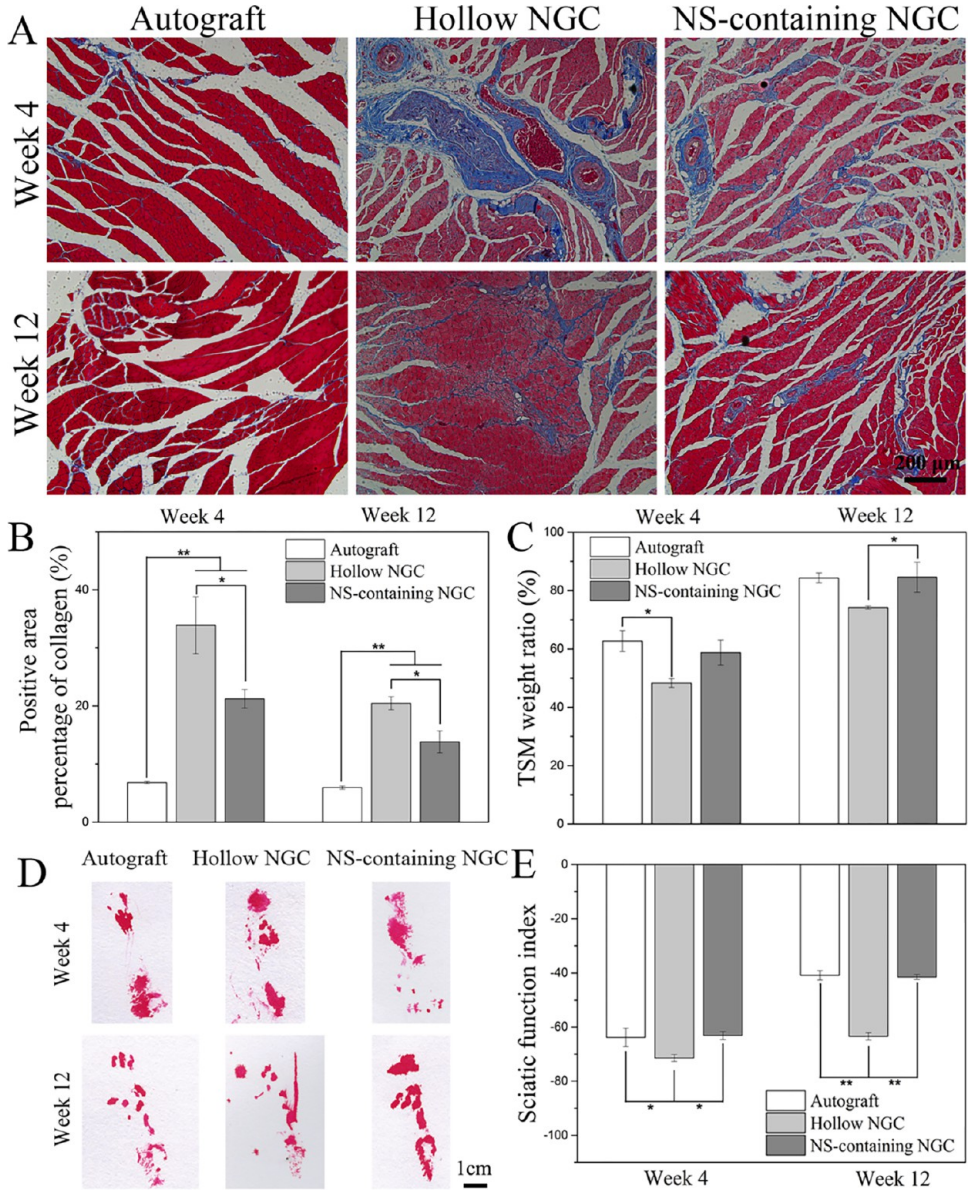

Figure 7. (A) Masson staining images of TSMs (experimental side) and (B) statistical results of collagen positive area percentage after implantation for 4 and 12 weeks. (C) TSMs weight ratio statistical results. (D) Footprints (experimental side) and (E) SFI statistical results of SD rats after surgery.

DOI: 10.1021/acsami.7b06707
ACS Appl. Mater. Interfaces 2017, 9, 26684−26696

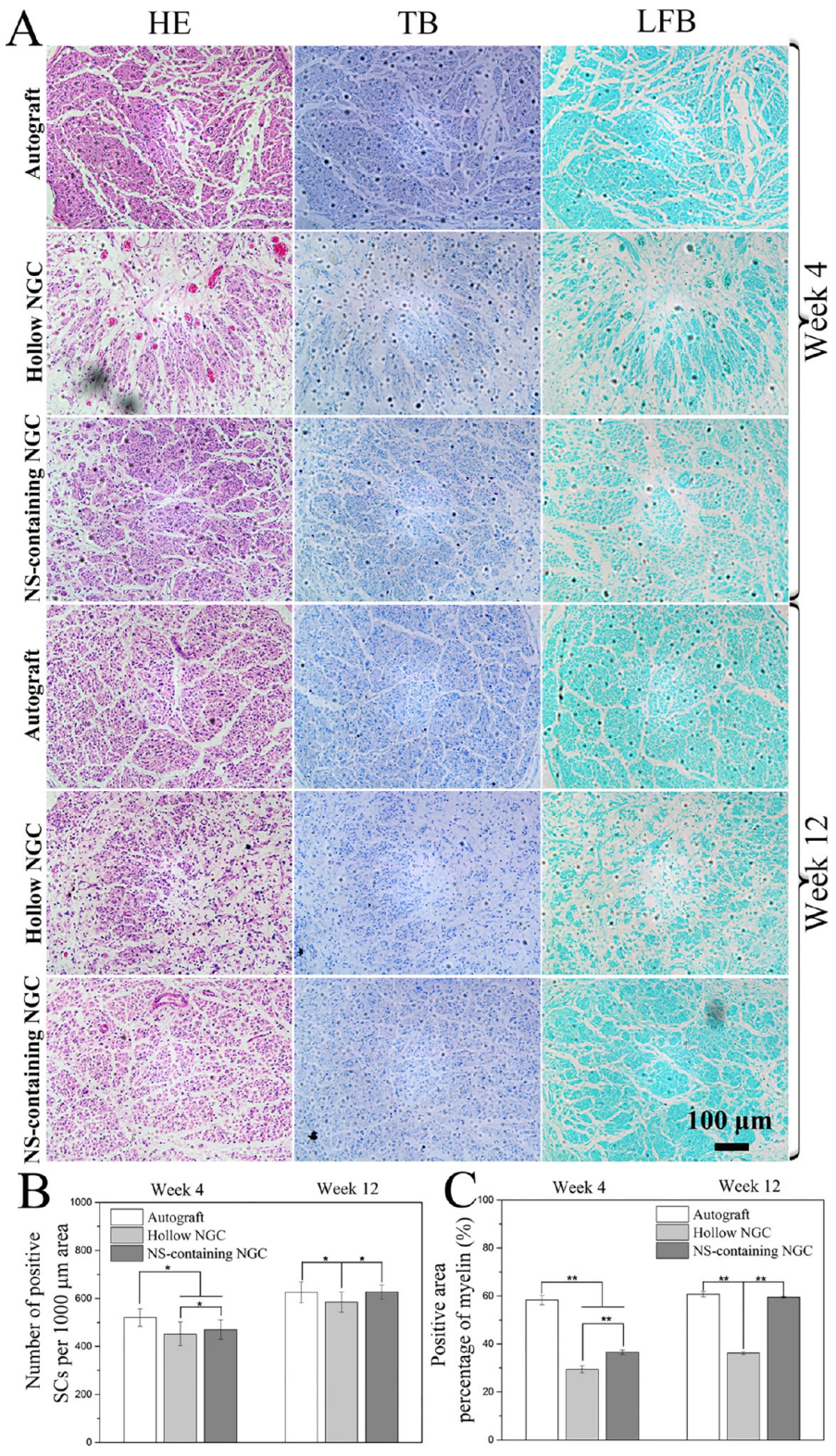

Figure 8. (A) HE, TB, and LFB staining images of the generated nerves at the middle segment of the NGCs (or autograft) after implantation for 4 and 12 weeks. (B) SCs density calculated by TB staining. (C) Positive area percentage of myelin calculated by LFB staining.

($P < 0.01$). However, there was no significant difference between NS-containing NGC and autograft groups.

3.7. Histological and Morphological Analysis. The autograft, hollow NGC, and NS-containing NGC were removed after being implanted for 4 and 12 weeks (Figure 6B). The regenerated nerve tissues were sectioned and stained with HE, TB, and LFB for histological and morphological analyses, respectively (Figure 8). HE and TB staining results revealed that there were lots of regenerated nerves and SCs in the implanted NGCs and autograft. No visible inflammation was observed (Figure 8A). LFB staining results indicated that numerous bunches of nerve myelin were produced in all nerve

DOI: 10.1021/acsami.7b06707
ACS Appl. Mater. Interfaces 2017, 9, 26684−26696

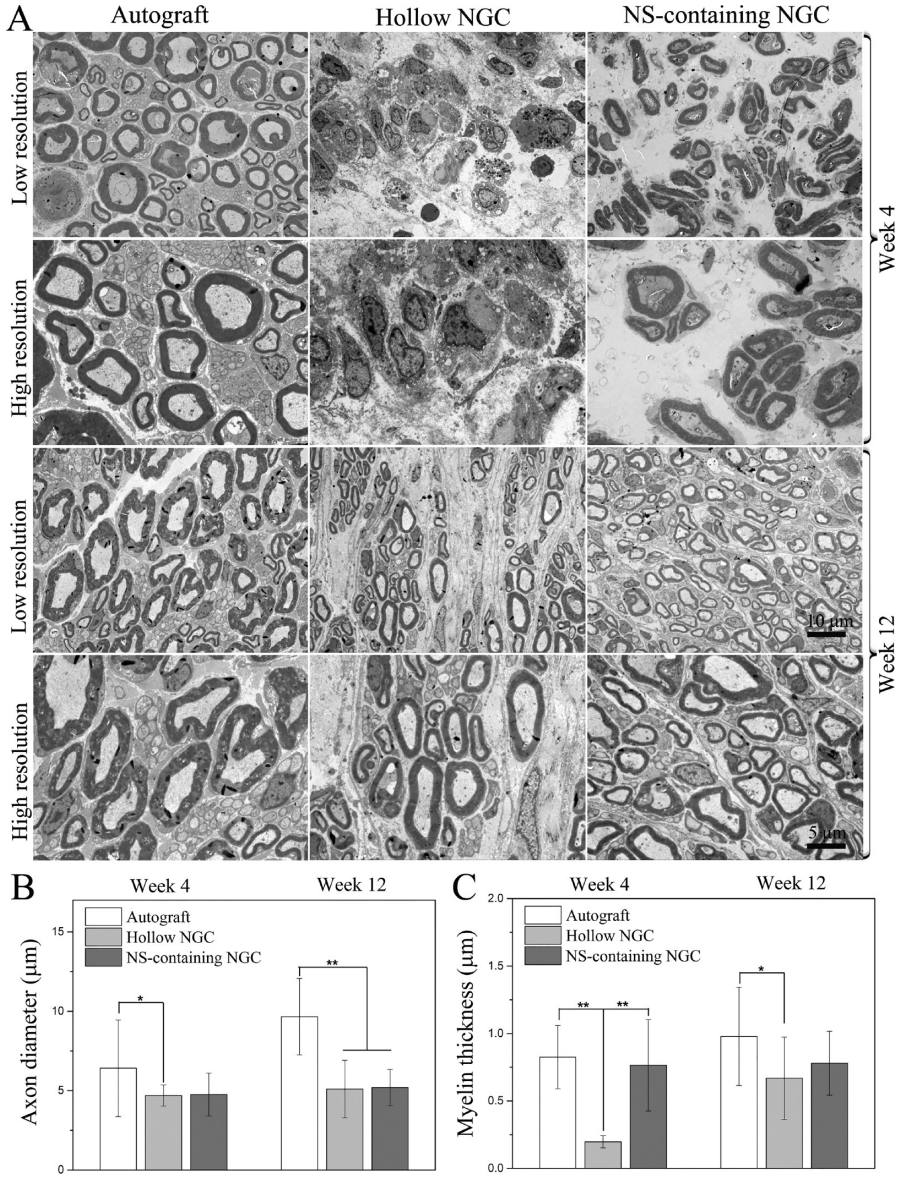

Figure 9. (A) TEM images of the generated nerves at the middle segment of the NGCs (or autograft) after implantation for 4 and 12 weeks. (B) Axon diameter and (C) myelin thickness calculated by TEM.

NGC groups and the autograft group. The density of positive SCs was calculated by TB staining images (Figure 8B), and quantitative results exhibited a higher density of SCs on NS-containing NGC group than hollow NGC ($P < 0.05$). Twelve weeks after implantation, the density of positive SCs on the NS-containing NGC group was close to that of the autograft group. The positive area percentage of myelin was calculated by LFB staining images as well (Figure 8C), which showed results similar to those with TB staining.

Additionally, TEM images are applied on the sections of the midportion of regenerated nerve after 4 and 12 weeks of implantation to evaluate the axon diameter and myelin thickness of regenerative axons (Figure 9). The general observation confirmed that the regenerated axon and myelin were generated in all of the groups (Figure 9A). In addition, it showed that more myelinated nerve fibers were regenerated on NS-containing NGC than hollow NGC. The statistical results indicated that there was no significant difference in the axon diameter between hollow NGC group and NS-containing NGC. However, differences were found in consideration to myelin thickness (Figure 9B,C). It is indicated that the myelin thickness of NS-containing NGC was significantly higher than the hollow NGC group at week 4 ($P < 0.01$), but close to the autograft group.

3.8. Immuno-histochemistry and Immunofluorescence. To evaluate the nerve repair of autograft and NGCs, three kinds of immuno-histochemistry (which are named NF-200, GFAP, and S-100) were presented (Figure 10A). The gross observations indicated that the positive expressions of three kinds of proteins were found in all tissues, though there were some differences among various groups. The quantitative analyses (Figure 10B) demonstrated the accurate assessment. For the S-100 index, the NS-containing NGC group showed an approximate positive area in comparison with the autograft group, and significantly higher than the hollow NGC group on weeks 4 ($P < 0.01$) and 12 ($P < 0.05$). For NF-200 and GFAP indexes, although the positive area of NS-containing NGC group was smaller than that of the autograft group, this value

DOI: 10.1021/acsami.7b06707
ACS Appl. Mater. Interfaces 2017, 9, 26684−26696

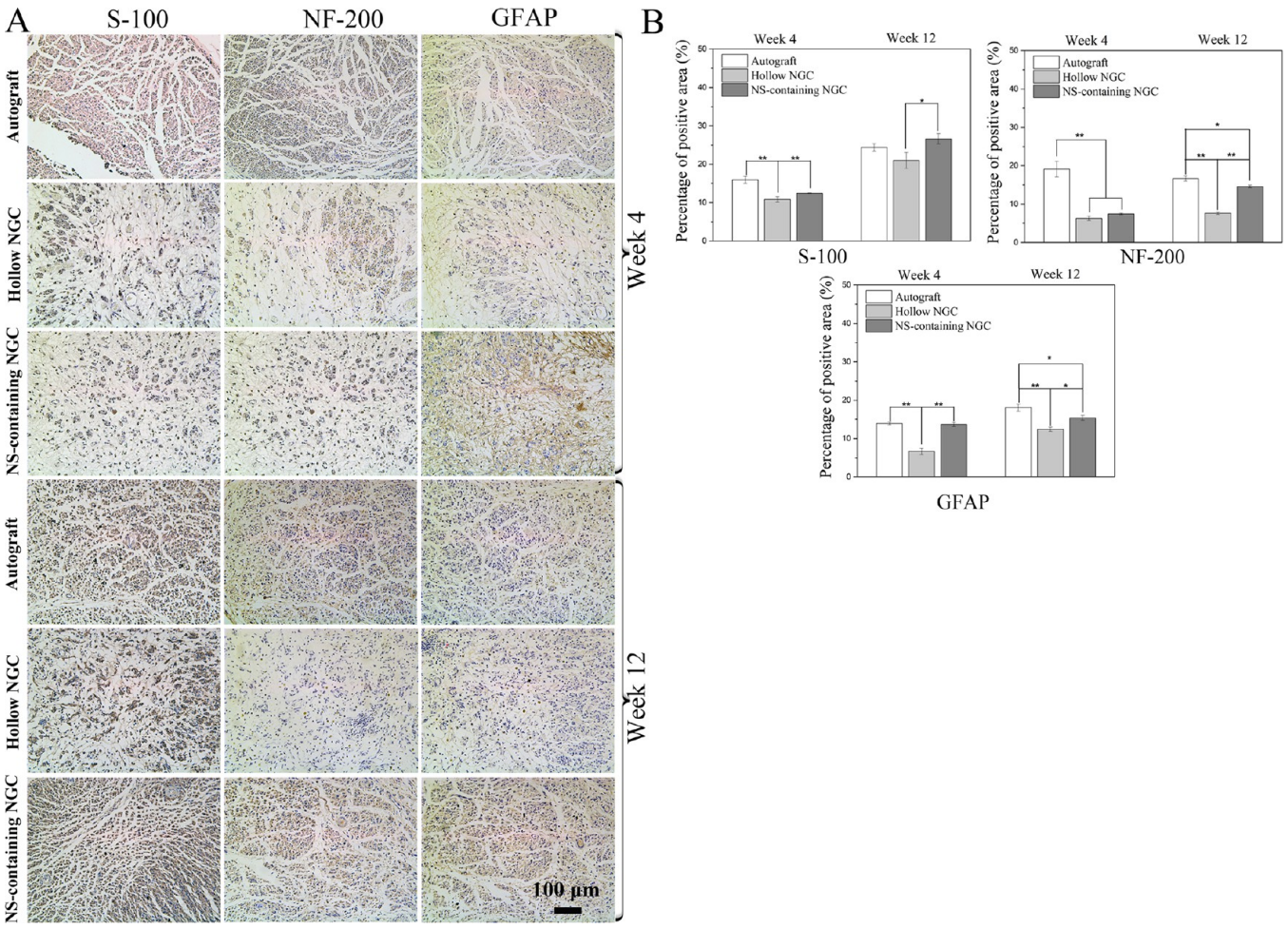

Figure 10. (A) Immuno-histochemical staining of S-100, NF-200, and GFAP in the regenerative tissue of different groups at 4 and 12 weeks postsurgery. (B) Relative positive area percentage of S-100, NF-200, and GFAP.

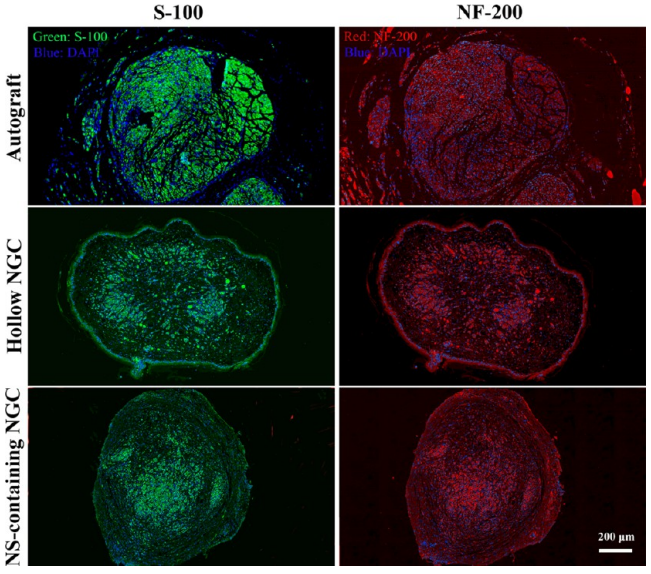

Figure 11. Immunofluorescence staining (indexes: S-100 and NF-200) images of regenerated nerves after implanted NGC (or autograft) at 4 weeks postsurgery.

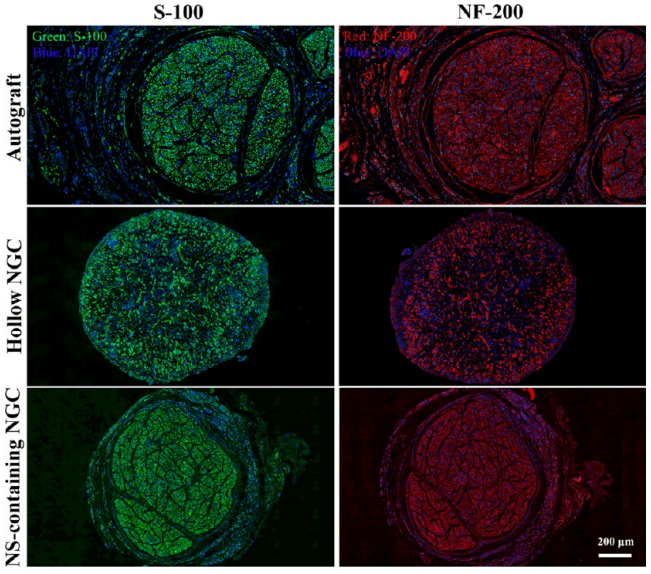

Figure 12. Immunofluorescence staining (indexes: S-100 and NF-200) images of regenerated nerves after implanted NGC (or autograft) at 12 weeks postsurgery.

was much higher than that of the hollow NGC group. Thus, it is confirmed that the nerve tissue showed better histological regeneration in NS-containing NGC than hollow NGC.

In addition, Figure 11 and Figure 12 showed the immunofluorescence staining images of regenerated nerves after 4 and 12 weeks of implantation, respectively. The regenerated nerves

DOI: 10.1021/acsami.7b06707
ACS Appl. Mater. Interfaces 2017, 9, 26684−26696

of all groups were observed with low and high (the inset images) resolutions, and the colors of green and red represent S-100 and NF-200 protein, respectively. The results were similar to the above-mentioned tests, which documented that the histological recoveries of regenerated nerves in the NS-containing NGC group were better than the hollow NGC group, but approximate to the gold standard autograft group.

4. DISCUSSION

It is a challenge to prepare 3D electrospun nanofiber scaffolds with high porosity and interconnected macropores for tissue engineering.[30] To address this problem, a 3D electrospun nanofiber scaffold was developed with high-speed dispersion and freeze-drying technology. These scaffolds were sponge-like with high porosity and compressive mechanical properties.[22] To prepare more appropriate nerve tissue engineering scaffold, PLCL and SF with good biocompatibility and biodegradability were used to fabricate nanofiber sponges. At first, PLCL/SF nanofiber membranes were prepared, which were subsequently dispersed and freeze-dried to generate nanofiber sponges. Then, PLCL/SF 3D nanofiber sponges were cross-linked with glutaraldehyde vapor (Figure 1). The nanofiber sponge scaffolds were cross-linked to became insoluble, which could also strengthen the scaffolds to bear more compression. Compared to PLCL/SF nanofiber membrane, the freeze-dried 3D nanofiber sponges and PLCL/SF 3D nanofiber sponges showed much higher porosity with larger pores ($P < 0.01$). Lots of interconnected macropores were found in freeze-dried nanofiber sponges (most of the pore sizes ranged from 50 to 300 μm) and PLCL/SF 3D nanofiber sponges (more of the pore size is from 10 to 100 μm), and the pore size of PLCL/SF nanofiber membrane was in the range of 0.5−12 μm (Figure 2). Therefore, the macropores on PLCL/SF 3D nanofiber sponges were large enough and beneficial for nutrient transport, especially for cell communication and infiltration. In addition, the PLCL/SF 3D nanofiber sponges showed good compressive elasticity properties even after 100 times compression (Figure 2). It was concluded that these 3D nanofiber sponges could maintain the porous structure for tissue engineering application.

Previous study showed that the filler-contained NGC had the mimicking structure of nerve fascicles, which was used to reduce the dispersion of regenerating axons for nerve tissue engineering.[6,14] In this study, cross-linked PLCL/SF 3D nanofiber sponges were used as NGC filler to fabricate NS-containing NGC, which had high porosity and compressive mechanical properties. The SEM results presented that PLCL/SF nanofiber sponges were filled into hollow NGC which kept its macropores structures (Figure 3). The results of CCK-8 assay indicated that SCs showed significantly better proliferation behaviors on NS-containing NGC than hollow NGC and TCP (Figure 4). In addition to good biocompatibility, the nanofiber sponge's existence could also provide more adhesion matrix for cells. It is necessary to note that whether SCs could infiltrate into the NS-containing NGC or not has been an evaluation standard for its application for nerve repair.[31] Herein, SCs were seeded on the NS-containing NGC and cultured for in vitro study (Figure 5). Immunofluorescence and HE staining results indicated that cells had superior adhesion and infiltration into the nanofiber sponges after culturing for 7 days, mainly due to the abundant macropores in NS-containing NGC. These in vitro results suggested that the NS-containing NGC could significantly improve the SCs proliferation and infiltration into the nanofiber sponges thanks to the high porosity and larger pores.

Consistent with in vitro results, the in vivo results also indicated that the developed NS-containing NGC were more advantageous for nerve repair and regeneration in a SD rat nerve defect model. It was observed that the defect nerve was rebridged after implantation of the autologous nerve and NGCs for both 4 and 12 weeks (Figure 6). However, the neural function recovery and nerve regeneration results of three groups (the group of autograft, hollow NGC, and NS-containing NGC) were different (Figure 7). To demonstrate the nerve function recovery of NGCs groups, TSM of the defect nerve's target organ was sectioned for Masson staining. The images and quantitative analysis demonstrated that more collagen was deposited in hollow NGC group than NS-containing NGC, i.e., the more serious loss of nerve function in hollow NGC which led to more severe myophagism and a greater amount of collagen enrichment. At the same time, the TSM weight ratio of all animals was calculated, which drew the same conclusions. SFI value is another important evaluation index for nerve function recovery. The SFI value of NS-containing NGC group was significantly higher than the hollow NGC group but close to the autograft group. This remarkable difference between NS-containing NGC and hollow NGC suggested that the existence of nanofiber sponges improved the recovery of nerve functions.

Histological and morphology evaluation of HE, TB, and LFB staining was performed (Figure 8). It was revealed that both hollow NGC and NS-containing NGC could guide nerve to rebridge after 4 or 12 weeks of implantation. No obvious inflammation was found during nerve regeneration. PLCL/SF nanofiber was dispersed to fabricate nanofiber sponges which provide a biomimic ECM environment for SCs growth and axons elongation. SCs density and myelin area were calculated by TB and LFB staining, respectively. The NS-containing NGC group exhibited obviously higher SCs density and remyelination compared with the hollow NGC after being implanted for 4 weeks ($P < 0.05$). Furthermore, after 12 weeks of implantation, this difference increased ($P < 0.01$). It was suggested that the guidance of NS-containing NGC for nerve regeneration might be reflected from the first month. TEM results showed the diameter and myelin thickness of regenerative axons (Figure 9). It was well-known that the regeneration of peripheral neural started with the SCs adhesion and proliferation on NGC matrix.[6] Therefore, providing more matrixes for SCs adhesion and proliferation when nerve was injured could promote axons elongation and nerve regeneration. Immuno-histochemistry of NF-200, GFAP, and S-100 were characterized to evaluate the nerve tissues' regenerates as superior markers (Figure 10). NF-200 is an important intermediate filament in neurons. The functions of NF-200 include structural support and regulation of axons regeneration. Besides, NF-200 is an essential marker for the mature axons.[32] GFAP is another protein which is an important component for nerve cells' cytoskeletal reorganization, myelination maintenance, and cell adhesion.[33] S-100 protein normally presents neurotrophic effects in the central and peripheral nervous system.[34] Thus, during the process of nerve regeneration, the detecting of S-100 protein was used to evaluate SCs proliferation and migration. These results manifested that the defect nerve was regenerated in all the NGCs and autograft group at the histological level. However, more proteins were expressed on NS-containing NGC than hollow NGC group. Such results demonstrated the nanofiber sponges in the NGC

DOI: 10.1021/acsami.7b06707
ACS Appl. Mater. Interfaces 2017, 9, 26684−26696

were suitable for tissue repairing. Additionally, observation from the immunofluorescence indicated NS-containing NGC group showed a better recovery of neural nutrition and axon maturation (Figures 11 and 12).

In vivo results confirmed better nerve regenerated guidance with NS-containing NGC than hollow NGC. The nanofiber sponges in NGC promote SCs proliferation and axons outgrowth. In the report of Cai et al., it was mentioned that few SCs were found in the center region of hollow NGC than filaments-containing NGC. Also SCs were difficult to migrate to the distal regions without containing filaments.[11,35] This was consistent with the observation from our study. In addition, most of the studies on the filler-containing NGC were focused on the orientated fibers, filaments, and gels, because nerve tissues have the structure of axial orientation in bionics.[36,37] In this study, the filler of NGC was random nanofiber sponges, which successfully bridged the 10 mm gap in the rat model. Our results demonstrate that nanofiber sponges could also guide SCs migrating and promote nerve regeneration through the lumen of the conduit. On one hand, this may be due to the NS-containing NGC having large pores to accommodate the SCs infiltration and proliferation. On the other hand, the balance between supporting density and space occupation of the NS-containing NGC was very important for nerve regeneration.[11] In this study, the nanofiber sponges had a faster degradation rate to match the nerve regeneration rate. It was estimated reabsorption of NS-containing in vivo would take about 1−3 months to complete, although degradation tests were not mentioned in this study. In summary, our experimental results suggested that the newly developed 3D nanofiber sponges containing NGC could provide a more favorable microenvironment for nerve regeneration, although the detailed mechanisms might still need to be further investigated.

5. CONCLUSIONS

In the present study, nanofiber sponges were fabricated via electrospinning and freeze-drying. Morphology characterization indicated that the PLCL/SF 3D nanofiber sponges consisted of nanofiber with macroporous structure. The pore size was higher than 10 μm, and the porosity was 88.81 ± 1.13%, which was much higher than the PLCL/SF nanofiber membranes. Meanwhile, mechanical experiments confirmed that the PLCL/SF 3D nanofiber sponges could still maintain high elasticity after 100 compression tests. In comparison with hollow NGC, in vitro study indicated that SCs cultured on NS-containing NGC showed better proliferation, which might be contributed to the infiltration of cells in the macropores of NS-containing NGC. The evaluation of nerve functional recovery showed that TSMs of NS-containing NGC had more serious atrophy than hollow NGC. The SFI value of NS-containing NGC was lower than hollow NGC, close to that of autograft group. Furthermore, through the evaluation of histology and morphology, immuno-histochemistry, and immunofluorescence, it was surprising to find that more SCs, axons, and thicker myelin were regenerated on NS-containing NGC compared with hollow NGC. In summary, the NS-containing NGC not only successfully bridged the sciatic nerve defect of SD rats but also showed a better repair effect than hollow NGC for peripheral nerve injury.

AUTHOR INFORMATION

Corresponding Authors

*Email: xmm@dhu.edu.cn (X.M.).
*E-mail: eastpool@alumni.sjtu.edu.cn (Y.Y.).

ORCID

Hany El-Hamshary: 0000-0001-6805-7255
Xiumei Mo: 0000-0002-8717-856X

Notes

The authors declare no competing financial interest.

ACKNOWLEDGMENTS

This research was supported by the National Key Research Program of China (Grant No. 2016YFA0201702 of 2016YFA0201700), the National Nature Science Foundation of China (Grant Nos. 31470941 and 31271035), the Science and Technology Commission of Shanghai Municipality (Grant Nos. 15JC1490100 and 15441905100), and the Yantai Double Hundred Talent Plan and the Opening Project of State Key Laboratory of Polymer Materials Engineering (Sichuan University) (Grant No. sklpme2016-4-29). This was also supported by the Fundamental Research Funds for the Central Universities (Grant Nos. CUSF-DH-D-2017046 and CUSF-DH-D-2017047). We extend our sincere appreciation to the Deanship of Scientific Research at King Saud University for its funding through the Research Group Project No. RGP-201.

REFERENCES

(1) Noble, J.; Munro, C. A.; Prasad, V. S.; Midha, R. Analysis of Upper and Lower Extremity Peripheral Nerve Injuries in a Population of Patients with Multiple Injuries. *J. Trauma* **1998**, *45*, 116−122.
(2) Robinson, L. R. Traumatic Injury to Peripheral Nerves. *Muscle Nerve* **2000**, *23*, 863−873.
(3) Taylor, C. A.; Braza, D.; Rice, J. B.; Dillingham, T. The Incidence of Peripheral Nerve Injury in Extremity Trauma. *Am. J. Phys. Med. Rehabil.* **2008**, *87*, 381−385.
(4) Yucel, D.; Kose, G. T.; Hasirci, V. Polyester Based Nerve Guidance Conduit Design. *Biomaterials* **2010**, *31*, 1596−1603.
(5) Kehoe, S.; Zhang, X. F.; Boyd, D. Fda Approved Guidance Conduits and Wraps for Peripheral Nerve Injury: A Review of Materials and Efficacy. *Injury* **2012**, *43*, 553−572.
(6) Gu, X.; Ding, F.; Williams, D. F. Neural Tissue Engineering Options for Peripheral Nerve Regeneration. *Biomaterials* **2014**, *35*, 6143−6156.
(7) de Ruiter, G. C.; Spinner, R. J.; Malessy, M. J. A.; Moore, M. J.; Sorenson, E. J.; Currier, B. L.; Yaszemski, M. J.; Windebank, A. J. Accuracy of Motor Axon Regeneration across Autograft, Single Lumen, and Multichannel Poly(Lactic-Co-Glycolic Acid) Nerve Tubes. *Neurosurgery* **2008**, *63*, 144−155.
(8) Hu, X.; Huang, J.; Ye, Z.; Xia, L.; Li, M.; Lv, B.; Shen, X.; Luo, Z. A Novel Scaffold with Longitudinally Oriented Microchannels Promotes Peripheral Nerve Regeneration. *Tissue Eng., Part A* **2009**, *15*, 3297−3308.
(9) Brushart, T. M.; Mathur, V.; Sood, R.; Koschorke, G. M. Dispersion of Regenerating Axons across Enclosed Neural Gaps. *J. Hand Surg. Am.* **1995**, *20*, 557−564. (1994 Recipient of the Joseph H. Boyes Award.)
(10) Matsumoto, K.; Ohnishi, K.; Kiyotani, T.; Sekine, T.; Ueda, H.; Nakamura, T.; Endo, K.; Shimizu, Y. Peripheral Nerve Regeneration across an 80-Mm Gap Bridged by a Polyglycolic Acid (Pga)-Collagen Tube Filled with Laminin-Coated Collagen Fibers: A Histological and Electrophysiological Evaluation of Regenerated Nerves. *Brain Res.* **2000**, *868*, 315.
(11) Cai, J.; Peng, X.; Nelson, K. D.; Eberhart, R.; Smith, G. M. Permeable Guidance Channels Containing Microfilament Scaffolds Enhance Axon Growth and Maturation. *J. Biomed. Mater. Res., Part A* **2005**, *75*, 374−386.
(12) Dubey, N.; Letourneau, P. C.; Tranquillo, R. T. Guided Neurite Elongation and Schwann Cell Invasion into Magnetically Aligned Collagen in Simulated Peripheral Nerve Regeneration. *Exp. Neurol.* **1999**, *158*, 338−350.

DOI: 10.1021/acsami.7b06707
ACS Appl. Mater. Interfaces 2017, 9, 26684−26696

(13) Lundborg, G.; Kanje, M. Bioartificial Nerve Grafts. A Prototype. *Scand. J. Plast. Reconstr. Surg. Hand Surg.* **1996**, *30*, 105−110.
(14) Chew, S. Y.; Mi, R.; Hoke, A.; Leong, K. W. Aligned Protein-Polymer Composite Fibers Enhance Nerve Regeneration: A Potential Tissue-Engineering Platform. *Adv. Funct. Mater.* **2007**, *17*, 1288−1296.
(15) Yang, F.; Murugan, R.; Wang, S.; Ramakrishna, S. Electrospinning of Nano/Micro Scale Poly(L -Lactic Acid) Aligned Fibers and Their Potential in Neural Tissue Engineering. *Biomaterials* **2005**, *26*, 2603−2610.
(16) Sill, T. J.; von Recum, H. A. Electrospinning: Applications in Drug Delivery and Tissue Engineering. *Biomaterials* **2008**, *29*, 1989−2006.
(17) Sun, B.; Long, Y. Z.; Zhang, H. D.; Li, M. M.; Duvail, J. L.; Jiang, X. Y.; Yin, H. L. Advances in Three-Dimensional Nanofibrous Macrostructures Via Electrospinning. *Prog. Polym. Sci.* **2014**, *39*, 862−890.
(18) Wang, K.; Xu, M.; Zhu, M.; Su, H.; Wang, H.; Kong, D.; Wang, L. Creation of Macropores in Electrospun Silk Fibroin Scaffolds Using Sacrificial Peo-Microparticles to Enhance Cellular Infiltration. *J. Biomed. Mater. Res., Part A* **2013**, *101*, 3474−3481.
(19) Xu, T.; Miszuk, J. M.; Zhao, Y.; Sun, H.; Fong, H. Electrospun Polycaprolactone 3d Nanofibrous Scaffold with Interconnected and Hierarchically Structured Pores for Bone Tissue Engineering. *Adv. Healthcare Mater.* **2015**, *4*, 2238−2246.
(20) Wang, X.; Ding, B.; Li, B. Biomimetic Electrospun Nanofibrous Structures for Tissue Engineering. *Mater. Today* **2013**, *16*, 229−241.
(21) Chen, W.; Ma, J.; Zhu, L.; Morsi, Y.; Ei-Hamshary, H.; Al-Deyab, S. S.; Mo, X. Superelastic, Superabsorbent and 3d Nanofiber-Assembled Scaffold for Tissue Engineering. *Colloids Surf., B* **2016**, *142*, 165−172.
(22) Chen, W.; Chen, S.; Morsi, Y.; El-Hamshary, H.; El-Newhy, M.; Fan, C.; Mo, X. Superabsorbent 3d Scaffold Based on Electrospun Nanofibers for Cartilage Tissue Engineering. *ACS Appl. Mater. Interfaces* **2016**, *8*, 24415−24425.
(23) Zhang, K.; Wang, H.; Huang, C.; Su, Y.; Mo, X.; Ikada, Y. Fabrication of Silk Fibroin Blended P(LLA-CL) Nanofibrous Scaffolds for Tissue Engineering. *J. Biomed. Mater. Res., Part A* **2010**, *93*, 984−993.
(24) Wang, C. Y.; Zhang, K. H.; Fan, C. Y.; Mo, X. M.; Ruan, H. J.; Li, F. F. Aligned Natural-Synthetic Polyblend Nanofibers for Peripheral Nerve Regeneration. *Acta Biomater.* **2011**, *7*, 634−643.
(25) Correia, C.; Bhumiratana, S.; Yan, L. P.; Oliveira, A. L.; Gimble, J. M.; Rockwood, D.; Kaplan, D. L.; Sousa, R. A.; Reis, R. L.; Vunjak-Novakovic, G. Development of Silk-Based Scaffolds for Tissue Engineering of Bone from Human Adipose-Derived Stem Cells. *Acta Biomater.* **2012**, *8*, 2483−2492.
(26) Sun, B.; Wu, T.; Wang, J.; Li, D.; Wang, J.; Gao, Q.; Bhutto, M. A.; El-Hamshary, H.; Al-Deyab, S. S.; Mo, X. Polypyrrole-Coated Poly(L-Lactic Acid-Co-E-Caprolactone)/Silk Fibroin Nanofibrous Membranes Promoting Neural Cell Proliferation and Differentiation with Electrical Stimulation. *J. Mater. Chem. B* **2016**, *4*, 6670−6679.
(27) Serra, I. R.; Fradique, R.; Vallejo, M. C.; Correia, T. R.; Miguel, S. P.; Correia, I. J. Production and Characterization of Chitosan/Gelatin/Beta-Tcp Scaffolds for Improved Bone Tissue Regeneration. *Mater. Sci. Eng., C* **2015**, *55*, 592−604.
(28) de Medinaceli, L.; Freed, W. J.; Wyatt, R. J. An Index of the Functional Condition of Rat Sciatic Nerve Based on Measurements Made from Walking Tracks. *Exp. Neurol.* **1982**, *77*, 634−643.
(29) Forssmann, W. G.; Pickel, V.; Reinecke, M.; Hock, D.; Metz, J. *Immunohistochemistry and Immunocytochemistry of Nervous Tissue*; Springer: Berlin, Heidelberg, 1981; p 55−70.
(30) Kim, G. H.; Kim, W. D. Highly Porous 3d Nanofiber Scaffold Using an Electrospinning Technique. *J. Biomed. Mater. Res., Part B* **2007**, *81*, 104−110.
(31) de Luca, A. C.; Terenghi, G.; Downes, S. Chemical Surface Modification of Poly-E-Caprolactone Improves Schwann Cell Proliferation for Peripheral Nerve Repair. *J. Tissue Eng. Regener. Med.* **2014**, *8*, 153−163.
(32) Posmantur, R.; Hayes, R. L.; Dixon, C. E.; Taft, W. C. Neurofilament 68 and Neurofilament 200 Protein Levels Decrease after Traumatic Brain Injury. *J. Neurotrauma* **1994**, *11*, 533−545.
(33) Eng, L. F. Glial Fibrillary Acidic Protein (Gfap): The Major Protein of Glial Intermediate Filaments in Differentiated Astrocytes. *J. Neuroimmunol.* **1985**, *8*, 203−214.
(34) Mata, M.; Alessi, D.; Fink, D. J. S100 Is Preferentially Distributed in Myelin-Forming Schwann Cells. *J. Neurocytol.* **1990**, *19*, 432−442.
(35) Cai, J.; Peng, X.; Nelson, K. D.; Eberhart, R.; Smith, G. M. Synergistic Improvements in Cell and Axonal Migration across Sciatic Nerve Lesion Gaps Using Bioresorbable Filaments and Heregulin-B1. *J. Biomed. Mater. Res.* **2004**, *69*, 247−258.
(36) Keskin, M.; Akbaş, H.; Uysal, O. A.; Canan, S.; Ayyldz, M.; Ağar, E.; Kaplan, S. Enhancement of Nerve Regeneration and Orientation across a Gap with a Nerve Graft within a Vein Conduit Graft: A Functional, Stereological, and Electrophysiological Study. *Plast. Reconstr. Surg.* **2004**, *113*, 1372.
(37) Hibbard, E. Orientation and Directed Growth of Mauthner's Cell Axons from Duplicated Vestibular Nerve Roots. *Exp. Neurol.* **1965**, *13*, 289−301.

DOI: 10.1021/acsami.7b06707
ACS Appl. Mater. Interfaces 2017, 9, 26684−26696